# Dual-activity PI3K–BRD4 inhibitor for the orthogonal inhibition of MYC to block tumor growth and metastasis

Forest H. Andrews[a,1], Alok R. Singh[b,c,1], Shweta Joshi[b,c,1], Cassandra A. Smith[d], Guillermo A. Morales[e], Joseph R. Garlich[e], Donald L. Durden[b,c,e,2,3], and Tatiana G. Kutateladze[a,d,2,3]

[a]Department of Pharmacology, University of Colorado School of Medicine, Aurora, CO 80045; [b]Division of Pediatric Hematology-Oncology, Department of Pediatrics, Moores Cancer Center, UC San Diego School of Medicine, La Jolla, CA 92130; [c]Rady Children's Hospital San Diego, San Diego, CA 92123; [d]Program in Structural Biology and Biochemistry, University of Colorado School of Medicine, Aurora, CO 80045; and [e]SignalRx Pharmaceuticals, Inc., San Diego, CA 92130

Edited by Haitao Li, Tsinghua University, Beijing, China, and accepted by Editorial Board Member Dinshaw J. Patel December 30, 2016 (received for review August 8, 2016)

***MYC* is a major cancer driver but is documented to be a difficult therapeutic target itself. Here, we report on the biological activity, the structural basis, and therapeutic effects of the family of multi-targeted compounds that simultaneously disrupt functions of two critical MYC-mediating factors through inhibiting the acetyllysine binding of BRD4 and the kinase activity of PI3K. We show that the dual-action inhibitor impairs PI3K/BRD4 signaling in vitro and in vivo and affords maximal MYC down-regulation. The concomitant inhibition of PI3K and BRD4 blocks *MYC* expression and activation, promotes MYC degradation, and markedly inhibits cancer cell growth and metastasis. Collectively, our findings suggest that the dual-activity inhibitor represents a highly promising lead compound for the development of novel anticancer therapeutics.**

MYC | bromodomain | BRD4 | PI3K | inhibitor

The *MYC* gene is frequently altered in human cancer. It encodes a transcription factor that binds to and regulates nearly 10–15% of genes in the human genome (1–3). The MYC targets mediate fundamental biological processes necessary for cell survival and general well-being, ranging from gene-expression and cell-cycle programs to cell proliferation and response to DNA damage, thereby establishing MYC as a global transcriptional regulator. *MYC* is overexpressed or amplified in many human cancers, which results in genome instability and deregulation of an array of signaling pathways responsible for malignant transformation. *MYC* expression level as well as synthesis, stability, and posttranslational modifications (PTMs) of the MYC protein are tightly regulated via several pathways, including PI3K–AKT–mTOR and RAS–MAPK (4). Particularly, PI3K activation blocks MYC degradation through inhibiting GSK3β-dependent MYC phosphorylation at threonine 58, elevating MYC levels and inducing MYC-dependent oncogenic programs (4, 5).

*MYC* gene expression has recently been linked to the activity of the BET (bromodomains and extraterminal domain) family of transcriptional coactivators (6–9). The BET protein BRD4 is found enriched at *MYC* and other oncogenes superenhancer and promoter regions, and transcriptional silencing of *MYC* coincides with the release of BET proteins from its locus, indicating that BET proteins can regulate *MYC* expression (10, 11). BRD4 itself is linked to multiple human malignancies: It forms chromosomal translocations in squamous carcinoma and NUT midline carcinoma, plays a role in progression of acute myeloid leukemia, and is up-regulated in breast cancer (7, 12–14). BRD4 contains a pair of bromodomains (BDs) that belong to the family of evolutionarily conserved structural modules that recognize acetyllysine PTMs in histones and nonhistone proteins (15, 16). Interestingly, BD1 and BD2 of BRD4 have distinct acetyllysine binding functions (17). BD1 binds to diacetylated histones, including histone H4 diacetylated at lysine 5 and lysine 8 (H4K5acK8ac), and this interaction helps to recruit or stabilize BRD4-containing transcription complexes at target gene promoters and enhancers. The second BD, BD2, selects for acetylated nonhistone proteins, though it is also capable of associating with acetylated histones H3 and H4. In the past few years, a number of BRD4-specific inhibitors have been developed, with some showing therapeutic effects in cancer models for NUT midline carcinoma, multiple myeloma, lymphoid leukemia, myeloid leukemia, and neuroblastoma (7, 8, 10, 12, 18–23).

Because MYC itself has been proven to be a difficult therapeutic target, the PI3K–AKT–mTOR pathway and inhibition of PI3K kinase activity in particular has been a main focus of drug development (4, 24). However, inhibition of PI3K to enhance degradation of MYC provides only a limited therapeutic effect and is often followed by the development of resistance to the drug (25). To overcome this problem and enhance efficacy, a combination of different inhibitors has been used as one of the treatment strategies. For example, combined PI3K and BET inhibition shows a beneficial antitumor effect in a model of metastatic breast cancer driven by PI3K and MYC (26). Likewise, BET inhibition suppresses transcription of a set of kinases, induced by the cancer drug Lapatinib, and prevents kinome adaptation, leading to a durable response to Lapatinib (27). A pioneering approach has been taken more recently to develop small-molecule compounds that can bind concomitantly to multiple targets, resulting in inhibition of more than one pathological pathway. Ciceri et al. have

## Significance

**In this work, we describe a dual-action inhibitor that simultaneously disrupts functions of two key MYC-mediating factors—PI3K and BRD4. We show that the concomitant inhibition of PI3K and BRD4 blocks *MYC* expression and activation, promotes MYC degradation, and markedly inhibits cancer cell growth and metastasis. Our findings suggest that the dual-activity inhibitor represents a highly promising lead compound for the development of novel anticancer therapeutics.**

Author contributions: F.H.A., A.R.S., S.J., D.L.D., and T.G.K. designed research; F.H.A., A.R.S., S.J., and C.A.S. performed research; F.H.A., A.R.S., S.J., C.A.S., G.A.M., J.R.G., D.L.D., and T.G.K. analyzed data; and F.H.A., S.J., D.L.D., and T.G.K. wrote the paper.

Conflict of interest statement: J.R.G., G.A.M., and D.L.D. are employees of SignalRx Pharmaceuticals and have financial conflicts of interest regarding the SF2523 compound and related compounds under study in this manuscript.

This article is a PNAS Direct Submission. H.L. is a Guest Editor invited by the Editorial Board.

Data deposition: Coordinates and structure factors have been deposited in the Protein Data Bank under accession codes 5U28, 5U2F, 5U2C, and 5U2E.

[1]F.H.A., A.R.S., and S.J. contributed equally to this work.

[2]D.L.D. and T.G.K. also contributed equally to this work.

[3]To whom correspondence may be addressed. Email: ddurden@ucsd.edu or Tatiana.Kutateladze@ucdenver.edu.

This article contains supporting information online at www.pnas.org/lookup/suppl/doi:10.1073/pnas.1613091114/-/DCSupplemental.



www.pnas.org/cgi/doi/10.1073/pnas.1613091114

screened a library of kinase inhibitors, including clinically approved drugs, and identified several compounds that interact with BRD4 with affinity in a nanomolar range (28). Dittmann et al. show that two compounds commonly used in cell biology assays to explore PI3K signaling or inflammatory consequences inhibit acetyllysine binding activity of BRD2, BRD3, and BRD4 (29).

Here, we report on the biological activity, the structural mechanism, and therapeutic effects of the family of dual-activity inhibitors that simultaneously disrupt the acetyllysine binding function of BRD4 and the kinase activity of PI3K. The dual-action inhibitor blocks MYC expression and activation, increases MYC degradation, markedly inhibits cancer-cell growth and metastasis, and represents a promising lead compound for the development of novel anticancer therapeutics.

## Results and Discussion

**Morpholinothienopyrane Is a Dual Inhibitor of PI3K and BRD4.** We have previously shown that 5-morpholino-7H-thieno[3,2-*b*]pyran-7-one (TP-scaffold) represents a promising class of PI3K inhibitors: Screening a panel of >200 kinases, we found that SF2523 is a highly selective and potent inhibitor of PI3K, particularly of the α isoform of PI3K (PI3Kα) (30). To assess SF2523 activity in the cellular context, we examined the effect of this compound on the PI3K signaling pathway in a neuroblastoma SKNBE2 cell line. We focused on the major established downstream effectors of the PI3K pathway—AKT and MYCN (one of the MYC family genes amplified in this cell line)—and evaluated levels and activation of these effectors. SKNBE2 cells were treated first with IGF and then with either SF2523 or known PI3K inhibitors, including SF1126, BKM120, BEZ235, and CAL101, and MYCN mRNA levels were measured by RT-PCR (Fig. 1*A*). Whereas all PI3K inhibitors tested significantly decreased *MYCN* expression, SF2523 had the most profound effect, reducing the MYCN mRNA level by ∼sevenfold. Western blot analysis of the SKNBE2 cell lysate revealed that SF2523 treatment decreases protein levels of MYCN and Cyclin D1, the *MYCN* target, and inhibits AKT activation by blocking phosphorylation of AKT at Ser473 (Fig. 1*B*). By contrast, other commonly used PI3K inhibitors, such as BKM120, BEZ235, and CAL101, blocked phosphorylation of AKT and slightly reduced MYCN levels but did not affect Cyclin D1 levels, implying that besides the PI3K signaling cascade, additional targets of SF2523 likely exist that could also regulate *MYCN* expression.

Because *MYC* transcription has been linked to the activity of the transcriptional coactivator BRD4 and several kinase inhibitors have been found to act on BRD4 (28, 29), we tested whether SF2523 targets BRD4. As anticipated, treatment of SKNBE2 cells with JQ1, a commonly used inhibitor of BRD4 that has no PI3K inhibitory activity, resulted in a decrease of *MYCN* expression and reduced MYCN and Cyclin D1 levels but had no effect on pAKT, indicating that JQ1 appears to not alter the PI3K–AKT signaling (Fig. 1 *A* and *B*). Further, chromatin immunoprecipitation (ChIP) experiments revealed that JQ1 displaces BRD4 from *MYCN* promoter sites (regions 1 and 2 within the *MYCN* promoter), and similarly to JQ1, SF2523 treatment led to the displacement of BRD4 from both *MYCN* promoter sites (Fig. 1*C*). Unlike JQ1 and SF2523, the PI3Kδ selective inhibitor CAL101 was unable to displace BRD4 from the *MYCN* promoter.

**BDs Are Targets of TP-Scaffold Inhibitors.** To determine whether SF2523 is capable of binding to BDs of BRD4, SF2523 was tested against a panel of BDs derived from 28 proteins in a BROMOscan binding assay. As shown in Fig. 1*D*, SF2523 interacts robustly with the full-length BRD4 ($K_d$ = 140 nM) and exhibits comparable affinity to the BRD4 first BD (BD1) ($K_d$ = 150 nM), however it binds more weakly to the second BD (BD2) of BRD4 ($K_d$ = 710 nM). Comparison of binding affinities of SF2523 for BDs of other proteins revealed that it binds equally well to BDs of BRD4, BRD2, and BRD3; shows moderate binding to BDs of CECR2 and BRDT; but associates much weaker with other BDs (Fig. 1*D* and Fig. S1). Binding affinities of SF2523 to BD1 and BD2 of BRD4 were corroborated by $K_d$ values measured by isothermal titration calorimetry (ITC) (Fig. 1 *E* and *F*). Such strong and selective binding of the PI3K-specific inhibitor to BRD2/3/4 appears to be unique, as none of the known PI3K inhibitors tested noticeably disrupted the interaction of BRD4 with its ligand, polyacetylated histone H4 peptide (H4K5acK8acK12acK16ac), in a kinase screening assay, whereas SF2523 had an $IC_{50}$ of 16 nM (Fig. 2*A* and Fig. S2). In contrast, displacement binding assays with H4K5acK8acK12acK16ac peptide showed that SF2523 is a robust inhibitor of acetyllysine binding activity of BRD4 BD1 ($IC_{50}$, 241 nM) and a moderate inhibitor of BD2 ($IC_{50}$, 1.5 μM) (Fig. 2 *A* and *B*).

The direct binding of SF2523 to BRD4 BD1 was substantiated by NMR $^{1}H,^{15}N$ heteronuclear single quantum coherence (HSQC) titration experiments (Fig. 2). Gradual addition of SF2523 to the $^{15}N$-labeled BRD4 BD1 NMR sample caused large chemical shift perturbations (CSPs) that are indicative of direct binding (Fig. 2*D*, *Left*). A slow exchange regime on the NMR time scale—that is, disappearance of a set of cross-peaks corresponding to the free state of the protein and appearance of another set of cross-peaks corresponding to the bound state—revealed a tight interaction, corroborating the nanomolar values of $K_d$ and $IC_{50}$.

In an attempt to increase inhibition potency, a second generation of the TP-scaffold compounds was tested in displacement binding assays (Fig. 2*B*). Of the five compounds tested, SF2558HA was found to be a slightly stronger inhibitor of BRD4 than SF2523, and unlike SF2523, which exhibits fivefold higher selectivity for BRD4 BD1, SF2558HA disrupted acetyllysine-binding function of both BD1 and BD2 almost equally well (Fig. 2 *B* and *C*). SF2535 demonstrated an increase of inhibition toward BRD4 BD2 and was also a potent inhibitor of another PI3K isoform, PI3Kδ ($IC_{50}$, 41 nM) (Fig. 2*A*). In further agreement with the displacement assay findings, titration of SF2558HA and SF2535 into the $^{15}N$-labeled BRD4 BD1 NMR samples resulted in similar patterns of CSPs in BD1, with the exception of a pair of side-chain amide cross-peaks, which are in the slow exchange regime upon binding of SF2523 but are in the fast exchange regime upon binding of SF2558HA and SF2535 (Fig. 2*D*). We concluded that the overall binding mode of the TP-scaffold compounds to BD1 is conserved; however, characterization of these interactions at the atomic resolution is necessary to better understand the differences in selectivity and potency of these inhibitors.

**Structural Mechanism for BRD4 BD1 Inhibition by TP Compounds.** To elucidate the molecular mechanism for inhibition of BRD4 BDs by the TP-scaffold compounds, we cocrystallized BRD4 BD1 with SF2523, SF2535, and SF2558HA and obtained crystal structures of the complexes. The structure of the BRD4 BD1–SF2523 complex reveals a characteristic four-helix bundle fold of BD1, with SF2523 occupying a deep hydrophobic pocket at one of the open ends of the bundle (Fig. 3*A* and Table S1). The morpholino and thienopyrano rings of SF2523 are inserted deeply in the pocket and lay parallel to the α-helices of BD1, whereas the benzodioxane moiety of SF2523 is positioned perpendicular to the α-helices and oriented toward the ZA loop of BD1. The carbonyl oxygen in the thienopyrano group of SF2523 forms a hydrogen bond with the amide nitrogen of Asn140 and a water-mediated hydrogen bond with the hydroxyl group of Tyr97 of BD1. The dioxane ring of SF2523 is restrained through a set of hydrogen bonds involving Trp81, Gln85, and Asp88 in the ZA loop of BD1. Side chains of Trp81, Pro82, and Leu92 create a hydrophobic cage around the benzodioxane group of SF2523, whereas the side chains of Val87 and Ile146 provide additional stabilization to the thiophene portion of SF2523 (Fig. 3*B*). The base of the binding pocket is lined with a well-defined and

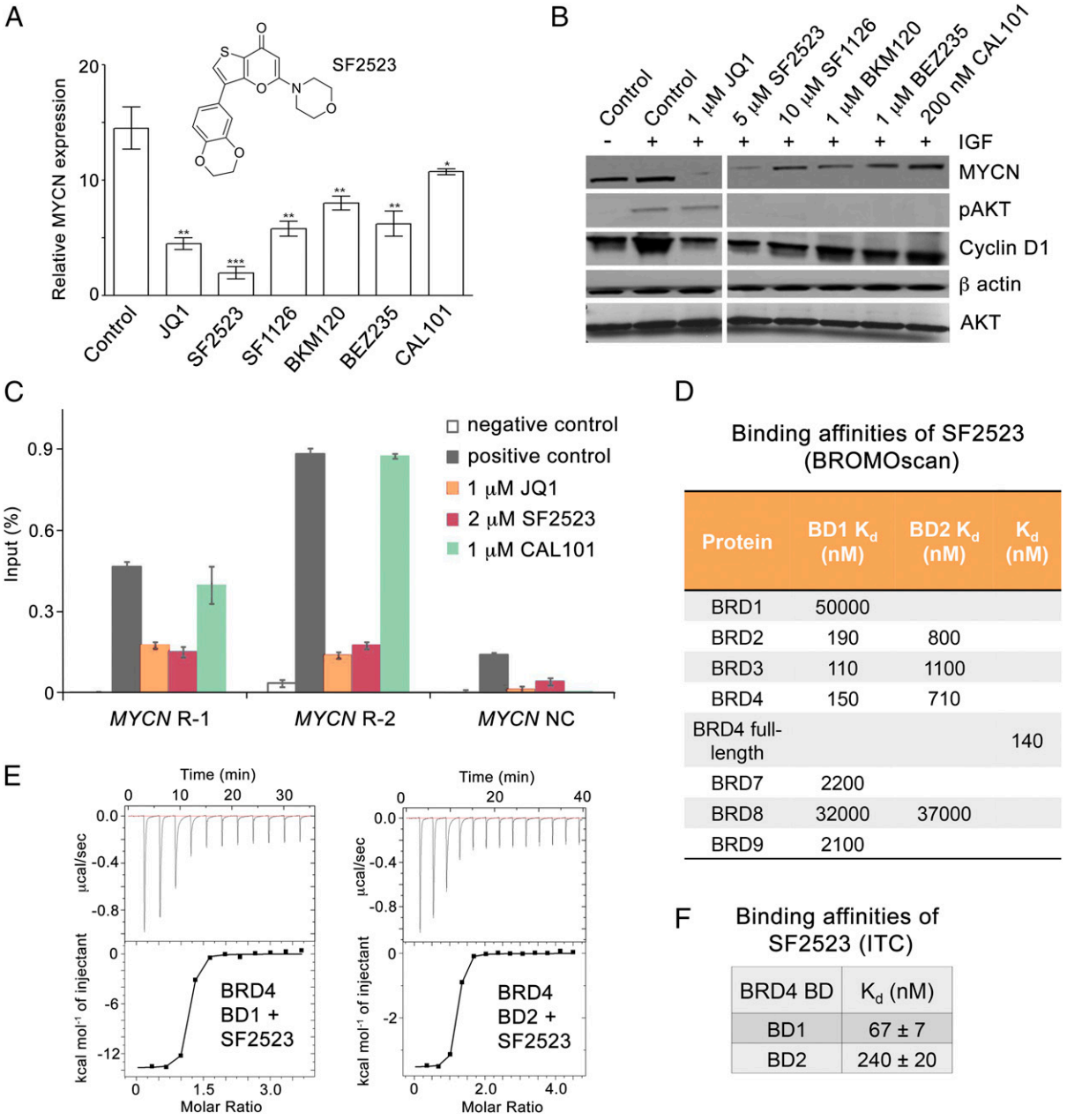


| Protein | BD1 $K_d$ (nM) | BD2 $K_d$ (nM) | $K_d$ (nM) |
|---|---|---|---|
| BRD1 | 50000 | | |
| BRD2 | 190 | 800 | |
| BRD3 | 110 | 1100 | |
| BRD4 | 150 | 710 | |
| BRD4 full-length | | | 140 |
| BRD7 | 2200 | | |
| BRD8 | 32000 | 37000 | |
| BRD9 | 2100 | | |

| BRD4 BD | $K_d$ (nM) |
|---|---|
| BD1 | 67 ± 7 |
| BD2 | 240 ± 20 |

**Fig. 1.** PI3K-specific inhibitor targets BRD4. (*A*) RT-PCR data showing the effect of indicated inhibitors on *MYCN* expression in neuroblastoma SKNBE2 cells. SKNBE2 cells were serum-starved for 4 h, stimulated with 50 ng/mL IGF, and treated with 1 μM JQ1, 5 μM SF2523, 10 μM SF1126, 1 μM BKM120, 1 μM BEZ235, or 200 nM CAL101 for 24 h. The doses of kinase inhibitors were chosen according to their $IC_{50}$ in SKNBE2 cells. Error bars are ±SEM. Data were analyzed by Student's *t* test, where $*P < 0.05$, $**P < 0.01$, $***P < 0.001$ vs. ctrl (DMSO). The chemical structure of SF2523 is shown. (*B*) Western blot analysis of lysates from SKNBE2 cells treated with indicated inhibitors for 30 min. Cell lysates were probed with specified antibodies. (*C*) BRD4 ChIP analysis was performed at the two *MYCN* promoter sites [region (R)-1 and R-2] and one negative control site (NC) in SKNBE2 cells treated with indicated inhibitors. Error bars are ±SEM from triplicate experiments. $P < 0.05$ comparing positive control to SF2523 or JQ1 treated cells (paired *t* test). Positive control, no inhibitor, IP with anti-BRD4 antibody; negative control, no inhibitor, IP with rabbit IgG. (*D*) Binding affinities of SF2523 to indicated BDs as measured by a BROMOscan binding assay. (*E*) Representative ITC curves for binding of SF2523 to BRD4 BD1 and BD2. (*F*) Binding affinities of SF2523 to indicated BDs as measured by ITC. Error bars are ±SEM of at least three separate experiments.

constrained shell of water molecules. Comparison of the BRD4 BD1 complexes with SF2523 or with H4K5acK8ac reveals that SF2523 acts as an acetyllysine mimetic: It forms the hydrogen bond with Asn140, which is conserved in acetyllysine–BD complexes, and does not disturb the signature water shell in BD1 (Fig. 3*C*).

Structural overlay of the BD1–SF2535, BD1–SF2558HA, and BD1–SF2523 complexes shows a high degree similarity of the water-lined binding sites (Fig. 3 *D* and *E*). Much like in the BD1–SF2523 complex, the thienopyrano group in SF2535 and SF2558HA is restrained via a conserved pair of hydrogen bonds (to Asn140 and Tyr97 of BD1); however, unlike the dioxane group in SF2523, the ethylcarboxyl group in SF2535 and the hydroxylamino group in SF2558HA do not form direct or water-mediated hydrogen bonds with Gln85 and Asp88. Instead, the Trp81 residue in the BD1–SF2558HA complex (but not in BD1–SF2535) adopts a distinctive

A

| Inhibitor | PI3K $IC_{50}$ (nM) | BRD4 BD1 $IC_{50}$ (nM) | BRD4 BD2 $IC_{50}$ (nM) |
|---|---|---|---|
| SF2523 | 16 (α isoform) | 241 | 1,550 |
| SF2535 | 41 (δ isoform) | 277 | 628 |
| BKM120 | | no activity | no activity |

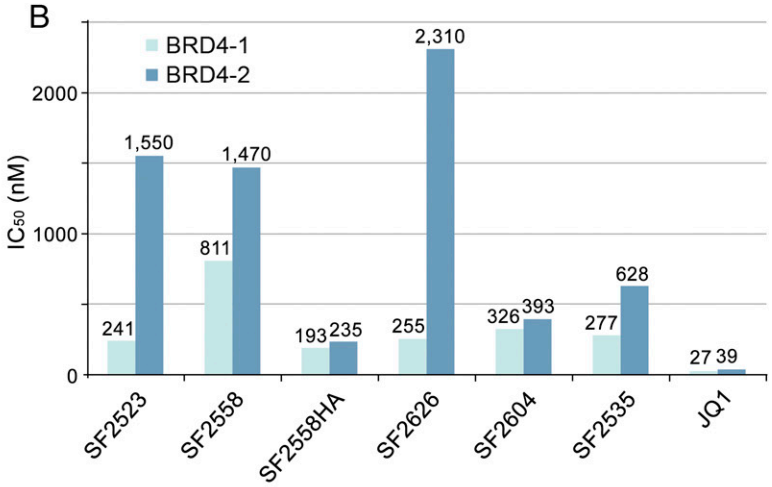


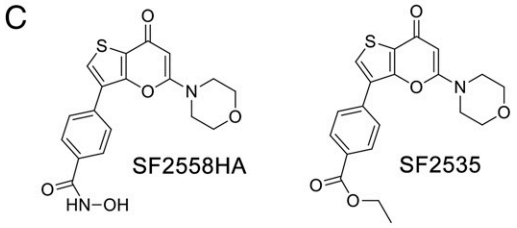


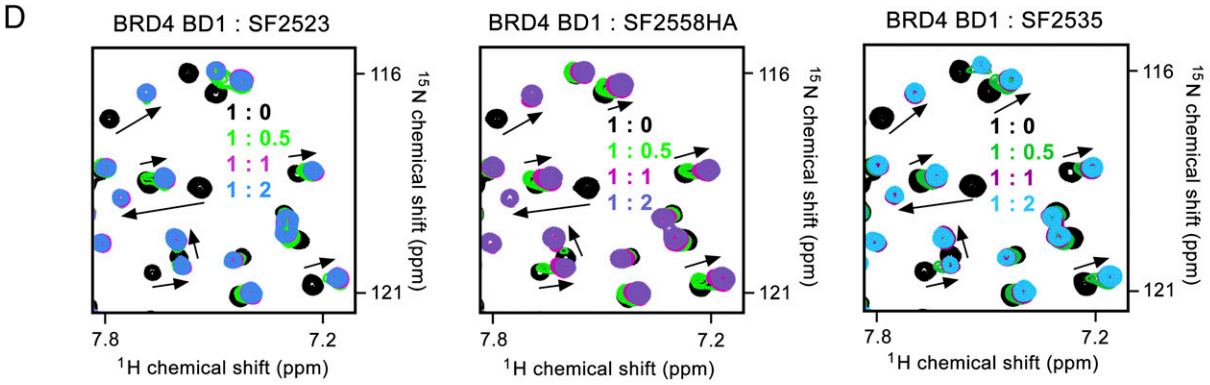


**Fig. 2.** Morpholinothienopyrane is an inhibitor of BDs. (*A* and *B*) $IC_{50}$ values, measured by displacement binding assays, show that SF2523 and its derivatives are inhibitors of BRD4 BDs. $IC_{50}$ values, measured by a kinase screening assay, are shown in the second column in *A*. (*C*) The chemical structures of SF2558HA and SF2535. (*D*) Superimposed $^{1}H$,$^{15}N$ HSQC spectra of uniformly $^{15}N$-labeled BRD4 BD1, recorded while the indicated inhibitors were titrated into the sample. The spectra are color-coded according to the protein:inhibitor molar ratio.



conformation, allowing for its indole nitrogen to make a transient hydrogen bonding contact with the hydroxylamino group of SF2558HA (Fig. 3*E*). Despite the differences in coordination of the thiophene substituent, the displacement and NMR titration experiments showed that the three compounds bind to BRD4 BD1 to a similar extent, suggesting that the morpholinothienopyrano core of these inhibitors plays a key role in the interaction with BD1, whereas the thiophene substituent can be varied to provide fine-tuned selectivity toward BD2.

**Intermolecular Contacts of the Thienopyranone Substituents Provide Selectivity.** To gain insight into the binding mode of BD2, we determined the crystal structure of BRD4 BD2 in complex with SF2558HA. In the complex, the SF2558HA molecule occupies the acetyllysine-binding pocket with the carbonyl group in the thienopyrano moiety positioned in close proximity to the side chains of Asn433 and Tyr390 and the morpholino oxygen being within a hydrogen-bonding distance to the imidazole nitrogen atom of His437 (Fig. 4*A*). Of the 18 residues within 5 Å of the bound SF2558HA compound, 15 are spatially conserved in BD2 and BD1. However, Gln85 in BD1, which forms a hydrogen bond with the dioxane ring of SF2523 in the BD1–SF2523 complex, is not conserved in BD2 (Fig. 4*B*). The inability of BD2 to form this stabilizing substituent contact could explain a ∼sixfold decrease in SF2523 activity toward BD2. On the contrary, Trp81 in BD1, which forms a hydrogen bond with the hydroxylamino group of SF2558HA but not with SF2523, is spatially conserved in BD2 (Trp374). Although the resolution of the BD2–SF2558HA structure precluded us to define the orientation of the Trp374 side chain, the capability of either BD to restrain the hydroxylamino group of SF2558HA through contact with tryptophan could explain a comparable activity of SF2558HA toward BD1 and BD2. In agreement, analysis of chemical shift changes in BD2 upon binding of the three inhibitors showed that although the majority of BD2 amide resonances, including resonances of residues that contribute to the stabilization of the TP-scaffold, were perturbed in a similar way, residues in the ZA loop of BD2 where Trp374 is located were perturbed differently (Fig. 4*C* and Fig. S3).

**TP Inhibitor Blocks Tumor Growth, Metastasis, and PI3K/BRD4 Signaling in Vivo.** Recent reports have shown that JQ1 suppresses growth of neuroblastoma in a set of in vivo models, including orthotopic transplantation of patient-derived xenografts and the TH-*MYC* mouse model (19, 31). To determine the therapeutic effects of the TP-scaffold inhibitors in aggressive neuroblastoma, we established an s.c. xenograft model of *MYCN*-amplified neuroblastoma in immunocompromised mice using the SKNBE2 cell line. Mice were randomized into two groups when tumors reached ∼100 $mm^3$ after 30 d of tumor implantation. One group was treated with vehicle (DMSO) and another with SF2523 (50 mg/kg, three times a week), until tumors were harvested. As shown in Fig. 5*A*, SF2523 treatment resulted in a significant reduction of tumor volume compared with tumor volume observed in the vehicle-treated group. Importantly, SF2523 showed no gross toxicity to the treated

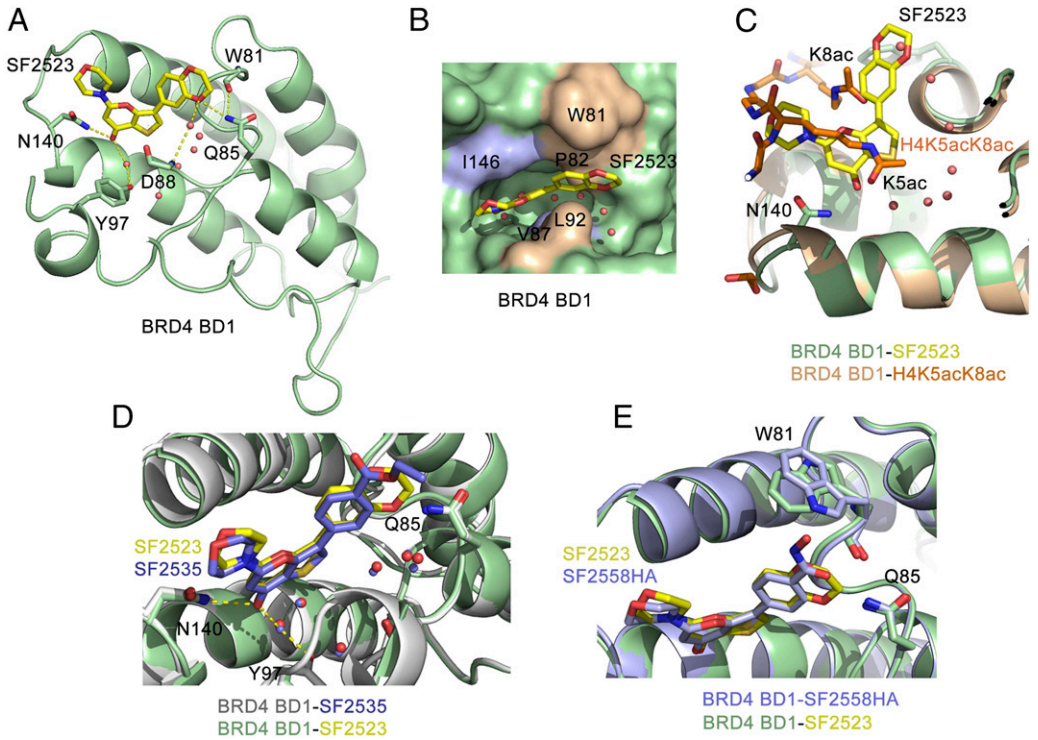


**Fig. 3.** Structural mechanism for the recognition of inhibitors by BRD4 BD1. (*A* and *B*) The crystal structure of BRD4 BD1 (green) in complex with SF2523 (yellow). Water molecules and hydrogen bonds are shown as yellow dashes and red spheres, respectively. (*C*) Overlay of the structures of BRD4 BD1 in complex with SF2523 (yellow) and H4K5acK8ac peptide (PDB ID code 3UVW) (orange). (*D*) Structural overlay of the complexes: BRD4 BD1 (green) with SF2523 (yellow) and BRD4 BD1 (gray) with SF2535 (blue), with water shells in these complexes shown as red and blue spheres, respectively. (*E*) Structural overlay of the complexes: BRD4 BD1 (green) with SF2523 (yellow) and BRD4 BD1 (light blue) with SF2558HA (light blue).

mice, as there was no notable change in body weight (Fig. 5*B*). These data demonstrate that SF2523 is highly efficacious in a high-risk *MYCN*-amplified neuroblastoma model.

We next assessed the ability of SF2523 to block PI3K activation and down-regulate *MYCN* and *Cyclin D1* in vivo. RT-PCR analysis of *MYCN* and *Cyclin D1* expression in tumors harvested from mice treated with SF2523 and from untreated animals revealed a significant decrease in both transcripts (Fig. 5*C*). Western blot analysis confirmed that tumors from SF2523-treated mice have markedly reduced MYCN, pAKT, and Cyclin D1 levels compared with levels of these proteins in vehicle-treated mice tumors (Fig. 5 *D* and *E*). Collectively, these results indicate that SF2523 targets PI3K-driven and BRD4-driven oncogenic pathways in vivo and in vitro (Figs. 1 *A* and *B* and 5 *C*–*E*).

Considering the role of PI3K and BRD4 signaling pathways in stimulation of tumor growth and metastasis (32–34), we examined the effects of SF2523 in the orthotopic pancreatic Panc02 carcinoma using a model for spontaneous lymph node metastasis. Furthermore, we compared the antitumor activities of SF2523 and two individual inhibitors combined, JQ1 and BKM120, to underscore the therapeutic benefit of the dual inhibition. For the spontaneous metastasis model, orthotopic pancreatic tumors were initiated by implanting Panc02 cells into the pancreas of C57BL/6 mice. At 20 d after tumor implantation, mice were randomized into four groups. One group ($n = 8$) was treated with 30 mg/kg of SF2523 formulated in 15% N,*N*-dimethylacetamide (DMA) and 30% captisol. The second group ($n = 8$) was treated with 30 mg/kg of JQ1 formulated in 30% captisol and 30 mg/kg of BKM120 formulated in 15% ethanol and 15% cremaphore. The other two groups ($n = 4$ for both) were used as controls and treated with either formulation of 15% DMA and 30% captisol, or 15% ethanol and 15% cremaphore. Vehicles or inhibitors were administered intraperitoneally, five times a week, until tumors were harvested on day 35 after tumor implantation.

As shown in Fig. 6 *A* and *B*, there was a drastic weight loss in animals treated with JQ1+BKM120, followed by death of four mice in this group. In addition, JQ1+BKM120-treated mice exhibited symptoms of hair loss. In contrast, the SF2523-treated group showed a very mild reduction in body weight with no mortality, and vehicle-treated mice showed neither weight loss nor mortality (Fig. 6 *A* and *B*). As expected, we observed a significant reduction of tumor growth in the Panc02 carcinoma model in mice treated with both SF2523 and JQ1+BKM120 ($P < 0.05$; Fig. 6 *C* and *D*). Because the Panc02 model is known to promote metastasis in lymph nodes, we investigated whether SF2523 treatment blocks metastasis in treated animals. Notably, mice orthotopically implanted with Panc02 cells in pancreas and treated with SF2523 displayed a marked reduction in regional colonic lymph node metastasis, and this effect was comparable to the effect of treatment with JQ1+BKM120 (Fig. 6 *E* and *F*). Altogether, these results suggest a high efficacy of SF2523 in controlling spontaneous lymph node metastasis.

## Concluding Remarks

An overwhelming amount of experimental data point to the direct link between cancer and deregulated PI3K–AKT signaling, rendering this signaling pathway into one of the most studied anticancer targets. Inhibition of PI3K has particularly become a highly desirable avenue for pharmacological intervention, with dozens of PI3K inhibitors, including taselisib, copanlisib, pictilisib, buparlisib, and others, being in clinical trials and idelasib being approved for a set of leukemias and lymphomas (4, 35). Although initially very promising, targeted inhibition of PI3K often suffers from the development of resistance to drugs. It has also been noticed that such resistance is associated with MYC up-regulation. This

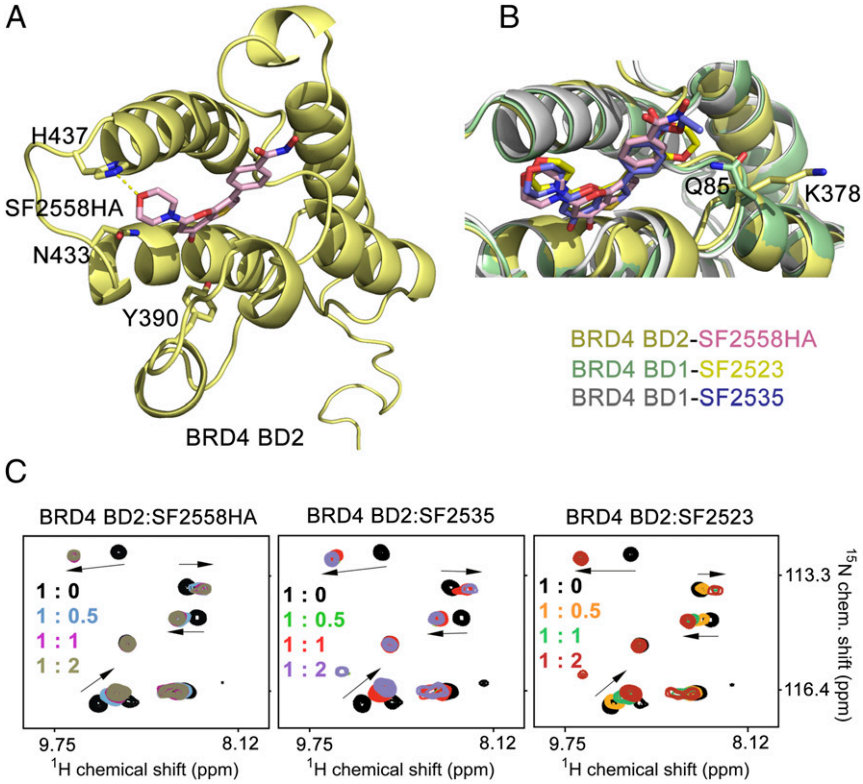


**Fig. 4.** Structural mechanism for the recognition of inhibitors by BRD4 BD2. (*A*) The crystal structure of BRD4 BD2 (yellow) in complex with SF2558HA (pink). (*B*) Structural overlay of the complexes: BRD4 BD2 (yellow) with SF2558HA (pink), BRD4 BD1 (green) with SF2523 (yellow), and BRD4 BD1 (gray) with SF2535 (blue). (*C*) Superimposed $^{1}H,^{15}N$ HSQC spectra of uniformly $^{15}N$-labeled BRD4 BD2, recorded while the indicated inhibitors were titrated into the sample. The spectra are color-coded according to the protein:inhibitor molar ratio.

observation clearly illustrates that targeting a single protein/pathway may not provide a long-lasting therapeutic effect because of the highly heterogeneous nature of cancer, in which multiple signaling cascades are impaired, and that alternative approaches with the focus on synergistic inhibition of more than one deregulated or compensating pathway have to be developed. Currently, a number of clinical trials are ongoing to apply PI3K inhibitors in combination with other drugs (35).

In this study, we report on multitargeted small-molecule compounds that bind to a pair of distinctive cancer-specific targets. We describe a highly potent dual-activity inhibitor of PI3K and BRD4. This compound provides maximal inhibition of the major cancer driver—MYC—because inhibition of PI3K promotes MYC degradation, and simultaneously, inhibition of BRD4 blocks *MYC* transcription. The dual-activity inhibitor is characterized by improved efficacy and toxicity: SF2523 is less toxic to the host organism in vivo than a combination of an equipotent PI3K inhibitor and BRD4 inhibitor. Our data demonstrate that the dual-activity inhibitor blocks PI3K/BRD4 signaling in vitro and in vivo and is highly potent in controlling tumor growth and spontaneous lymph node metastasis. Our structural analysis provides atomic-resolution guidance on further optimization of the TP-scaffold with the goal to increase anticancer efficacy of the compounds toward these two key oncogenic signaling pathways.

## Methods

**Tissue Culture, Cell Lines, and Reagents.** The human neuroblastoma cell line SKNBE2 was obtained from ATCC. The Panc02 cell line from C57BL/6 mice has been previously described (34). All cell lines were tested for mycoplasma contamination and grown in DMEM (Invitrogen) supplemented with 10% FBS, 2 mM glutamine, and 1% penicillin–streptomycin at 37 °C in a 5% $CO_2$ atmosphere. All cell lines were authenticated by short tandem repeat DNA profiling at the respective cell banks and were maintained as recommended by the suppliers. JQ1 was a gift from James Bradner, Dana-Farber Cancer Institute, Boston, MA. BEZ235 and CAL101 were from Selleck Chemicals. BKM120 was from Novartis. Antibodies specific for AKT and pAKT were obtained from Cell Signaling Technology. Normal rabbit IgG, protein A/G agarose beads, Cyclin D1, and MYC antibodies were from Santa Cruz Biotechnology, and anti-BRD4 antibody was obtained from Bethyl Laboratories. SF2523 and SF2535 were synthesized as described (30), and synthesis of SF2558HA will be reported elsewhere.

**Western Blotting.** For Western blots, $2 \times 10^6$ SKNBE2 cells were plated in 10-cm tissue culture dishes and were allowed to adhere overnight. The cells were then serum-starved for 4 h, stimulated with 50 ng/mL IGF, and used for lysate preparation after 30 min of treatment with 1 μM JQ1, 5 μM SF2523, 10 μM SF1126, 1 μM BKM120, 1 μM BEZ235, or 200 nM CAL101. Whole-cell lysates were prepared using RIPA buffer containing protease inhibitor mixture (Roche Molecular Biochemicals). Clarified lysates were resolved in 10% SDS/PAGE, transferred to PVDF membrane, and probed for different antibodies.

**RNA Extraction and RT-PCR.** SKNBE2 cells were serum-starved for 4 h, stimulated with 50 ng/mL IGF, and used after 24 h of treatment with 1 μM JQ1, 5 μM SF2523, 10 μM SF1126, 1 μM BKM120, 1 μM BEZ235, or 200 nM CAL101 inhibitors for RNA isolation. Total RNA was extracted using the Qiagen RNAeasy kit (Qiagen) and reverse-transcribed using iscript cDNA synthesis kit (Bio-Rad). Amplification of cDNA was performed with 1× SYBR green supermix (Bio-Rad) on an CFX96 Real time system (Bio-Rad). cDNAs were amplified using specific MYCN and Cyclin D1 primers. Primer sequences are available upon request. Data were normalized to GAPDH.

**ChIP.** SKNBE2 cells were treated with/without JQ1 (1 μM), SF2523 (2 μM), and CAL 101 (1 μM) for 24 h and then cross-linked using 1.1% formaldehyde, washed with PBS, and frozen at –80 °C. Antibody-conjugated beads were prepared by blocking 50 μL of protein A/G agarose beads with 0.5% BSA (wt/vol) followed by incubation with 6.25 μg of anti-BRD4 antibody and 5 μg of normal rabbit IgG. Cross-linked cells were lysed, washed, and sonicated essentially as described (10, 19). Sonicated lysates were supplemented with

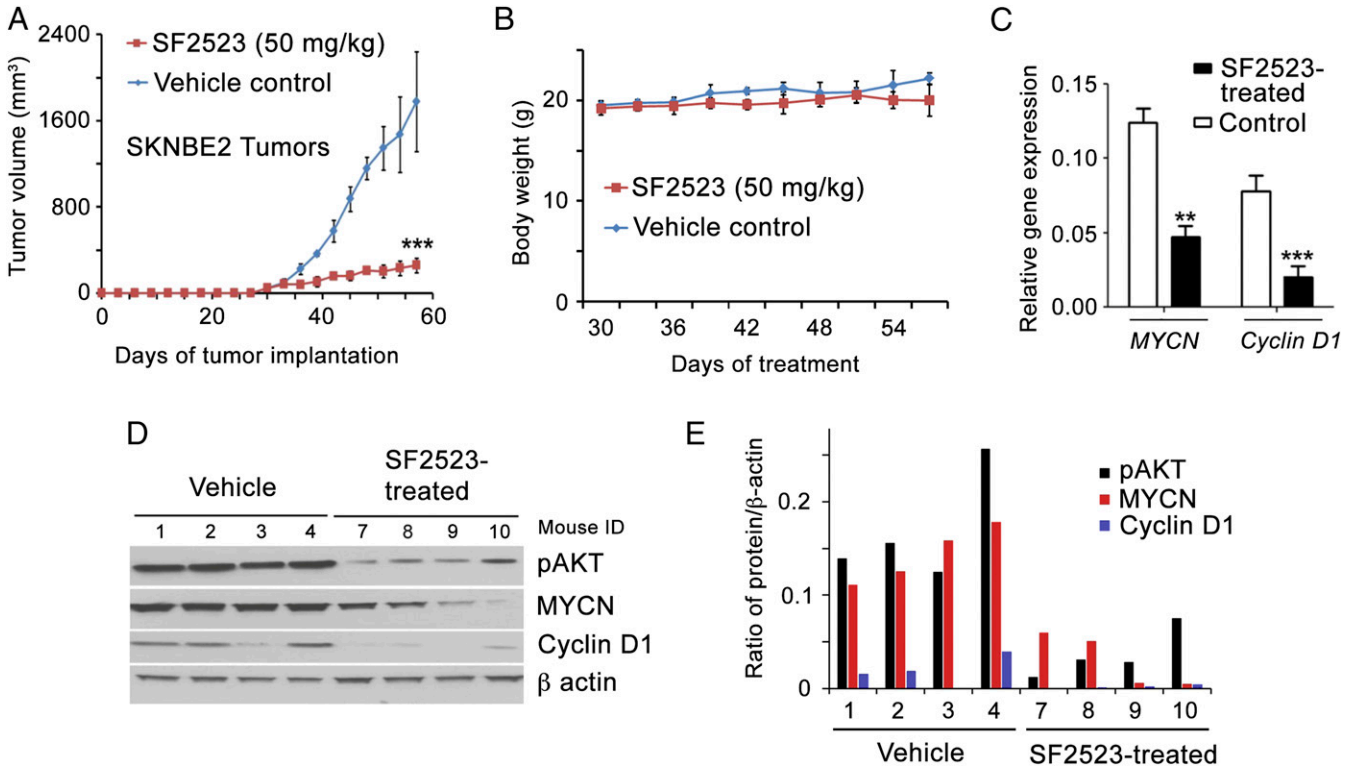


**Fig. 5.** SF2523 blocks tumor growth. (*A*) SKNBE2 cells were implanted in nude mice. When tumors reached ~100 $mm^3$ after 30 d of tumor implantation, animals were divided into two groups. One group was treated with vehicle (DMSO) and another with SF2523 (50 mg/kg, three times a week) until tumors were harvested. The number of mice per experimental group, $n = 6$. (*B*) The body weight of mice treated with SF2523 (50 mg/kg, 3 d a week). SF2523 shows no gross toxicity to mice, as there is no notable change in body weight. (*C*) RT-PCR data of *MYCN* and *Cyclin D1* from tumors isolated from *A*. (*D*) Levels of pAKT (Ser-473), MYCN, and Cyclin D1 analyzed by Western blot in the tumor tissues isolated from *A*. Tumors were harvested 4 h after the last treatment of 50 mg/kg SF2523. (*E*) Bands of pAKT, MYCN, CyclinD1, and β-actin in *D* were quantified using ImageJ software. pAKT, MYCN, and CyclinD1 protein expression levels were normalized to β-actin values. $^{**}P < 0.01$, $^{***}P < 0.001$.

Triton X-100 1% and cleared. Aliquots were reverse cross-linked and digested with RNase A overnight and purified with QIAquick PCR Purification Kit (Qiagen) for quantification of input chromatin. Sonicated, cleared chromatin (15 μg) was incubated overnight at 4 °C with antibody-conjugated agarose beads, and beads were washed as in refs. 10, 19. Chromatin was eluted in the buffer (50 mM Tris·HCl, pH 8, 10 mM EDTA, and 1% SDS), reverse cross-linked, and digested with RNase A overnight and then purified. ChIP and input DNA were analyzed by real-time PCR analysis using previously published primers against the *MYCN* promoter region 1, (forward) TTTGCACCTTCGGACTACCC and (reverse) TTTGACTGCGTGTTGTGCAG; *MYCN* promoter region 2, (forward) TCCTGGGAACTGTGTTGGAG and (reverse) TCCTCGGATGGCTACAGTCT; and *MYCN*-negative region, (forward) TATCACCGTCCATTCCCCG and (reverse) TTGGAGGCAGCTCAAAGACC (10, 19). Fold enrichment was analyzed by calculating the immunoprecipitated DNA percentage of input DNA in triplicate for each sample.

**Binding and Displacement Assays and Kinase Screening.** The $IC_{50}$ measurements for inhibition of BRD4 were performed by Reaction Biology using an Alpha screen assay on a set of His-tagged BDs and tetra-acetylated histone H4 peptide (1–21) (H4K5ac/8ac/12ac/16ac-Biotin) as a ligand. The $K_d$ measurements were performed by DiscoverX using the BROMOscan technology. PI3K activity screening and $IC_{50}$ measurements were performed by Life Technologies (Thermo Fisher Scientific) using ADAPTA, a fluorescence-based in vitro assay.

**ITC.** BRD4 BD1 and BD2 were buffer-exchanged into 10 mM Hepes (pH 7.5) supplemented with 1 mM TCEP and 100 mM NaCl via size-exclusion chromatography using an S100 column. ITC titrations were performed on the MicroCal iTC200 system (GE) at 25 °C. BD1 (0.5 mM) was titrated into 15 μM SF2523, and BD2 (2 mM) was titrated into 60 μM SF2523. Each titration was carried out until saturation via a series of successive injections (first at 0.2 μL and the remaining at 2 μL). Binding curves and heat plots were generated and processed using Origin 7.0 software (OriginLab). Error was calculated as the SE from at least three separate titrations.

**Protein Expression and Purification.** The BRD4 BD1 (amino acids 43–180) and BD2 (amino acids 342–460) constructs were expressed in *Escherichia coli* BL21 (DE3) RIL in either Luria Broth or M19 minimal media supplemented with $^{15}NH_4Cl$ and purified as GST fusion proteins. Cells were harvested by centrifugation and resuspended in 50 mM Hepes (pH 7.5) supplemented with 150 mM NaCl and 1 mM TCEP. Cells were lysed by freeze-thaw followed by sonication. Proteins were purified on glutathione Sepharose 4B beads, and the GST tag was cleaved with PreScission or thrombin protease.

**Crystallization and Structure Determination of BRD4 BD1 and BD2 Complexes.** BRD4 BD1 (amino acids 43–180) and BD2 (amino acids 342–460) were concentrated to 9–15 mg/mL in 10 mM Hepes (pH 7.5) supplemented with 100 mM NaCl and 1 mM TCEP and incubated with two molar equivalence of SF2523, SF2535, or SF2558HA on ice for 1 h before crystallization. All crystals were grown via sitting drop diffusion method. Crystals of BD1 in complex with SF2523 were grown at 4 °C by mixing 800 nL of protein/inhibitor solution with 800 nL of well solution composed of 40% PEG3350 (w/v) and 0.2 M potassium thiocyanate (pH 7.5). Crystals of BD1 SF2558HA and SF2535 complexes were obtained at 18 °C by combining 800 nL of protein/inhibitor solution with 800 nL of well solution comprised of 25% PEG3350 (w/v), 0.2 M ammonium chloride, and 0.1 M Tris (pH 8.5). Crystallization of the BD2 SF2558HA complex was achieved by mixing 800 nL of protein/ligand solution with 800 nL of well buffer composed of 2.5 M ammonium sulfate in 100 mM Tris (pH 7.5). All BD1 datasets were collected at 100 K on a Rigaku Micromax 007 high-frequency microfocus X-ray generator on a Pilatus 200K 2D area detector, and diffraction data for the BD2 SF2558HA complex were collected at 100 K on a "NOIR-1" detector system at the Molecular Biology Consortium Beamline 4.2.2 of the Advance Light Source (ALS). HKL3000 was used for indexing, scaling, and data reduction. Solution was found via molecular replacement with Phaser using BRD4 BD1 [Protein Data Bank (PDB) ID code 3MXF] or BRD4 BD2 (PDB ID code 2YEM) as search models with waters and ligands removed. Phenix was used for refinement of structures, and waters were manually placed using Coot.

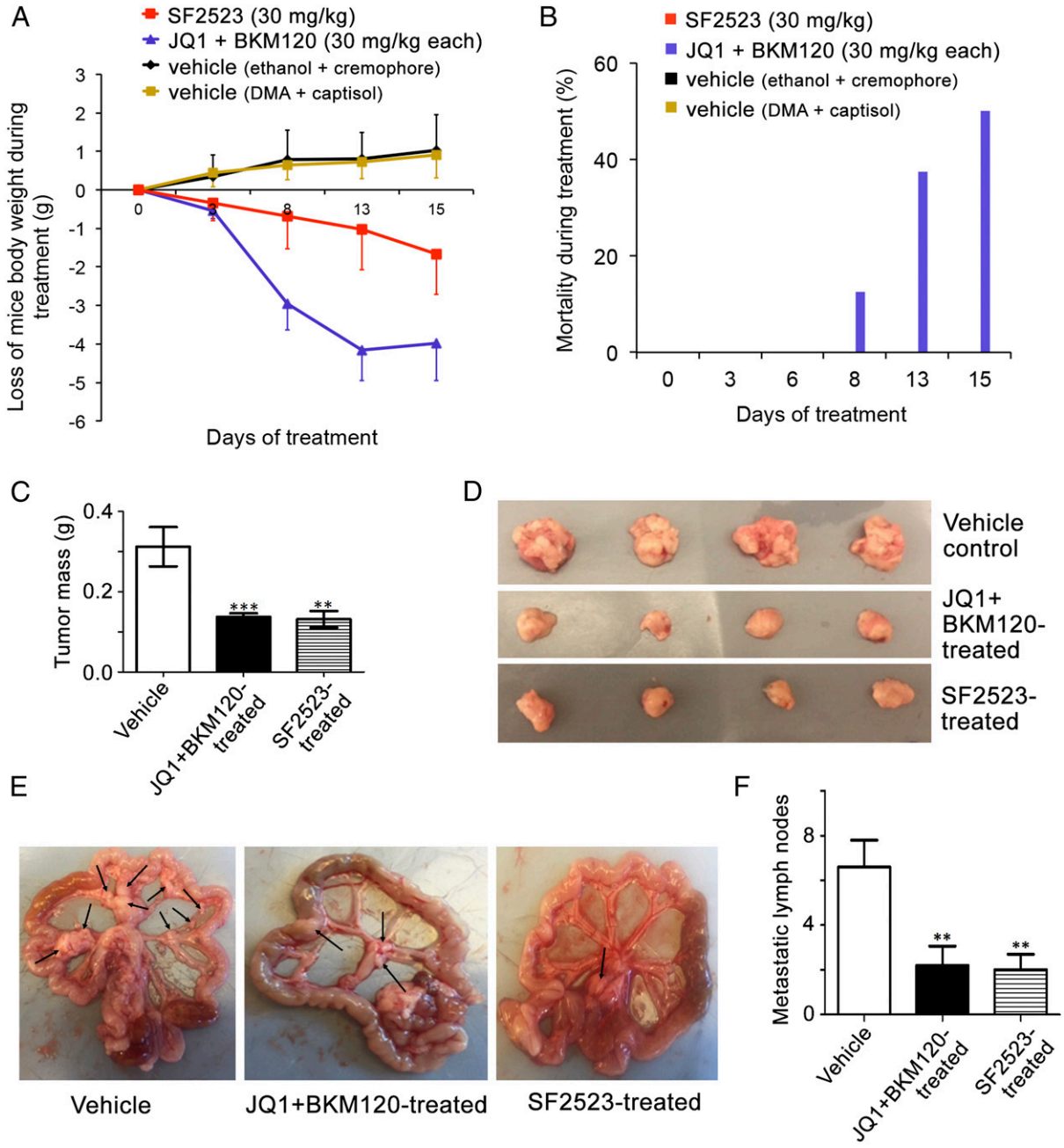


**Fig. 6.** SF2523 is efficacious in blocking tumor growth and metastasis. (*A*) Panc02 ($1 \times 10^6$) cells were injected in the pancreas of WT mice ($n = 24$). After 20 d of tumor implantation, mice were randomized into four groups and treated as described in *Results and Discussion*. Tumors were removed 35 d after tumor implantation. (*A*) Loss of mice body weight during treatment vs. day of treatment. Zero point represents the mice weight at the start of treatment. (*B*) Percentage of mortality of Panc02-implanted mice treated with 30 mg/kg of SF2523 or a combination of 30 mg/kg of JQ1 + 30 mg/kg of BKM120. (*C*) Tumor mass of pancreatic tumors implanted orthotopically in WT mice, treated with or without 30 mg/kg of SF2523 or a combination of 30 mg/kg of JQ1 + 30 mg/kg of BKM120. Values are mean ± SEM ($n = 8$; $^{**}P < 0.01$, $^{***}P < 0.001$; pair-wise two-sided Student's *t* test). (*D*) Representative images of pancreatic tumors isolated from pancreas of WT mice treated with either vehicle (control) or 30 mg/kg of SF2523 or a combination of 30 mg/kg of JQ1 + 30 mg/kg of BKM120. (*E*) Macroscopic view of Panc02 metastatic mesenteric lymph nodes from WT mice treated with either vehicle or 30 mg/kg of SF2523 or a combination of 30 mg/kg of JQ1 + 30 mg/kg of BKM120. (*F*) Number of metastatic mesenteric lymph nodes/mesentery observed in *E*. Values are mean ± SEM ($n = 8$; $^{**}P < 0.01$; pair-wise two-sided Student's *t* test).

**NMR Spectroscopy.** NMR spectroscopy was carried out on a Varian INOVA 600 MHz spectrometer outfitted with a cryogenic probe. CSP analysis was performed using uniformly $^{15}N$-labeled BRD4 BD1 or BRD4 BD2. The $^{1}H,^{15}N$ HSQC spectra of the BRD4 BD1 and BD2 were collected in the presence of increasing concentrations of either SF2523, SF2535, or SF2558HA in PBS buffer, pH 6.8, 8% $D_2O$.

**In Vivo Tumor Growth and Metastasis Experiments.** For in vivo efficacy studies, SKNBE2 cells ($2 \times 10^6$) were inoculated s.c. into nude mice (8 wk old, female, NSG) in the flank area, and tumor growth was monitored regularly. Tumor volume was calculated using the following formula: volume = (length × width$^2$)/2. When tumors reached a tumor volume of ~100 mm$^3$ after 30 d of tumor implantation, mice were randomized in two groups ($n = 6$ animals per group) and were treated intraperitoneally with vehicle (DMSO) or SF2523 (50 mg/kg, three times a week) until tumors were harvested.

For spontaneous metastasis, orthotopic pancreatic tumors were initiated by implanting $1 \times 10^6$ Panc02 into the pancreas of syngeneic mice as described before (34). After 20 d of tumor implantation, mice were treated

with either (*i*) 30 mg/kg of SF2523 formulated in 15% DMA + 30% captisol, (*ii*) 30 mg/kg of JQ1 formulated in 30% captisol in combination with 30 mg/kg of BKM120 formulated in 15% ethanol + 15% cremaphore, (*iii*) vehicle (15% ethanol + 15% cremaphore, as control), or (*iv*) another vehicle (15% DMA + 30% captisol, as control) five times a week, until tumors were removed on day 35. All procedures involving animals were approved by the University of California San Diego Animal Care Committee, which serves to ensure that all federal guidelines concerning animal experimentation were met.

**ACKNOWLEDGMENTS.** This work was supported by NIH Grants R01 GM101664, GM106416, and GM100907 (to T.G.K.) and R01 CA94233, STTR CA192646, and R01 FD04385 (to D.L.D.). F.H.A is supported by an AHA postdoctoral fellowship.

1. Meyer N, Penn LZ (2008) Reflecting on 25 years with MYC. *Nat Rev Cancer* 8(12): 976–990.
2. Dang CV (2012) MYC on the path to cancer. *Cell* 149(1):22–35.
3. Kress TR, Sabò A, Amati B (2015) MYC: Connecting selective transcriptional control to global RNA production. *Nat Rev Cancer* 15(10):593–607.
4. Dey N, Leyland-Jones B, De P (2014) MYC-xing it up with PIK3CA mutation and resistance to PI3K inhibitors: Summit of two giants in breast cancers. *Am J Cancer Res* 5(1):1–19.
5. Knoepfler PS, Kenney AM (2006) Neural precursor cycling at sonic speed: N-Myc pedals, GSK-3 brakes. *Cell Cycle* 5(1):47–52.
6. Nicodeme E, et al. (2010) Suppression of inflammation by a synthetic histone mimic. *Nature* 468(7327):1119–1123.
7. Filippakopoulos P, et al. (2010) Selective inhibition of BET bromodomains. *Nature* 468(7327):1067–1073.
8. Zhang G, Smith SG, Zhou MM (2015) Discovery of chemical inhibitors of human bromodomains. *Chem Rev* 115(21):11625–11668.
9. Filippakopoulos P, Knapp S (2014) Targeting bromodomains: Epigenetic readers of lysine acetylation. *Nat Rev Drug Discov* 13(5):337–356.
10. Delmore JE, et al. (2011) BET bromodomain inhibition as a therapeutic strategy to target c-Myc. *Cell* 146(6):904–917.
11. Mertz JA, et al. (2011) Targeting MYC dependence in cancer by inhibiting BET bromodomains. *Proc Natl Acad Sci USA* 108(40):16669–16674.
12. Zuber J, et al. (2011) RNAi screen identifies Brd4 as a therapeutic target in acute myeloid leukaemia. *Nature* 478(7370):524–528.
13. Crawford NP, et al. (2008) Bromodomain 4 activation predicts breast cancer survival. *Proc Natl Acad Sci USA* 105(17):6380–6385.
14. Shi J, et al. (2014) Disrupting the interaction of BRD4 with diacetylated Twist suppresses tumorigenesis in basal-like breast cancer. *Cancer Cell* 25(2):210–225.
15. Dhalluin C, et al. (1999) Structure and ligand of a histone acetyltransferase bromodomain. *Nature* 399(6735):491–496.
16. Filippakopoulos P, et al. (2012) Histone recognition and large-scale structural analysis of the human bromodomain family. *Cell* 149(1):214–231.
17. Gacias M, et al. (2014) Selective chemical modulation of gene transcription favors oligodendrocyte lineage progression. *Chem Biol* 21(7):841–854.
18. Dawson MA, et al. (2011) Inhibition of BET recruitment to chromatin as an effective treatment for MLL-fusion leukaemia. *Nature* 478(7370):529–533.
19. Puissant A, et al. (2013) Targeting MYCN in neuroblastoma by BET bromodomain inhibition. *Cancer Discov* 3(3):308–323.
20. Ran X, et al. (2015) Structure-based design of γ-carboline analogues as potent and specific BET bromodomain inhibitors. *J Med Chem* 58(12):4927–4939.
21. Zhang G, et al. (2013) Structure-guided design of potent diazobenzene inhibitors for the BET bromodomains. *J Med Chem* 56(22):9251–9264.
22. Zhao L, et al. (2015) Fragment-based drug discovery of 2-thiazolidinones as BRD4 inhibitors: 2. Structure-based optimization. *J Med Chem* 58(3):1281–1297.
23. Picaud S, et al. (2015) Generation of a selective small molecule inhibitor of the CBP/p300 bromodomain for leukemia therapy. *Cancer Res* 75(23):5106–5119.
24. Bendell JC, et al. (2012) Phase I, dose-escalation study of BKM120, an oral pan-Class I PI3K inhibitor, in patients with advanced solid tumors. *J Clin Oncol* 30(3):282–290.
25. Janku F, et al. (2012) PI3K/AKT/mTOR inhibitors in patients with breast and gynecologic malignancies harboring PIK3CA mutations. *J Clin Oncol* 30(8):777–782.
26. Stratikopoulos EE, et al. (2015) Kinase and BET inhibitors together clamp inhibition of PI3K signaling and overcome resistance to therapy. *Cancer Cell* 27(6):837–851.
27. Stuhlmiller TJ, et al. (2015) Inhibition of lapatinib-induced kinome reprogramming in ERBB2-positive breast cancer by targeting BET family bromodomains. *Cell Reports* 11(3):390–404.
28. Ciceri P, et al. (2014) Dual kinase-bromodomain inhibitors for rationally designed polypharmacology. *Nat Chem Biol* 10(4):305–312.
29. Dittmann A, et al. (2014) The commonly used PI3-kinase probe LY294002 is an inhibitor of BET bromodomains. *ACS Chem Biol* 9(2):495–502.
30. Morales GA, et al. (2013) Synthesis and cancer stem cell-based activity of substituted 5-morpholino-7H-thieno[3,2-b]pyran-7-ones designed as next generation PI3K inhibitors. *J Med Chem* 56(5):1922–1939.
31. Wyce A, et al. (2013) BET inhibition silences expression of MYCN and BCL2 and induces cytotoxicity in neuroblastoma tumor models. *PLoS One* 8(8):e72967.
32. Belkina AC, Nikolajczyk BS, Denis GV (2013) BET protein function is required for inflammation: Brd2 genetic disruption and BET inhibitor JQ1 impair mouse macrophage inflammatory responses. *J Immunol* 190(7):3670–3678.
33. Joshi S, Singh AR, Zulcic M, Durden DL (2014) A macrophage-dominant PI3K isoform controls hypoxia-induced HIF1α and HIF2α stability and tumor growth, angiogenesis, and metastasis. *Mol Cancer Res* 12(10):1520–1531.
34. Joshi S, et al. (2014) Rac2 controls tumor growth, metastasis and M1-M2 macrophage differentiation in vivo. *PLoS One* 9(4):e95893.
35. Massacesi C, et al. (2016) PI3K inhibitors as new cancer therapeutics: Implications for clinical trial design. *Onco Targets Ther* 9:203–210.